Progress in Oceanography 122 (2014) 116–130

Contents lists available at ScienceDirect

Progress in Oceanography

journal homepage: www.elsevier.com/locate/pocean

Seasonal dynamics in the Azores–Gibraltar Strait region: A climatologically-based study

L.I. Carracedo [a,*], M. Gilcoto [a], H. Mercier [b], F.F. Pérez [a]

[a] Marine Research Institute (IIM-CSIC), Eduardo Cabello 6, 36208 Vigo, Spain

[b] CNRS, Laboratoire de Physique des Océans, Institut Français de Recherche pour l'Exploitation de la Mer (IFREMER), Centre de Brest, C.S. 1007029280 Plouzané, France

ARTICLE INFO

Article history:
Received 4 March 2013
Received in revised form 17 December 2013
Accepted 22 December 2013
Available online 8 January 2014

ABSTRACT

Annual and seasonal mean circulations in the Azores–Gibraltar Strait region (North-Eastern Atlantic) are described based on climatological data. An inverse box model is applied to obtain absolute water mass transports consistent with the conservation of volume, salt and heat and the equations of the thermal wind. The large-scale gyre circulation (Azores Current, Azores Counter Current, Canary Current and Portugal Current) is well-represented in climatological data. The Azores Current annual mean transport was estimated to be 6.5 ± 0.8 Sv (1 Sv = 10^6 m^3/s) eastward, exhibiting a seasonal signal with minimum transport in the spring (5.3 ± 0.8 Sv) and maximum transport in autumn (7.3 ± 0.8 Sv). The Azores Current transport is twice that of the Azores Counter Current in spring and autumn and is four-times higher in summer and winter. The southward Portugal and Canary Currents show similar seasonal cycles with maximum transports in spring (3.5 ± 0.6 and 6.6 ± 0.4 Sv, respectively).

The overturning circulation within the area has an annual mean magnitude of 2.2 ± 0.1 Sv and two seasonal extremes; the highest in summer (2.6 ± 0.1 Sv) and the lowest in winter (1.7 ± 0.1 Sv). Of the annual mean, about two thirds (1.4 Sv) of the overturning circulation results from water mass transformation west of the Strait of Gibraltar: the downwelling and recirculation of upper Central Water (0.6 Sv) in the intermediate layer, the entrainment of Central Water (0.6 Sv) into the Mediterranean Outflow and the contribution of Antarctic Intermediate Water (0.2 Sv) to the Mediterranean Outflow. The remaining 0.8 Sv relates to the overturning in the Mediterranean Sea through the two-layer exchange at the Gibraltar Strait. Accordingly, the density level dividing the upper-inflowing and lower-outflowing limbs of the overturning circulation was found to be σ_1 = 31.65 kg m^{-3} (σ_1, potential density referred to 1000 db), which is above the isopycnal that typically separates Central and Mediterranean Water (σ_1 = 31.8 kg m^{-3}). In terms of water masses, we describe quantitatively the water mass composition of the main currents. Focusing on the spread of Mediterranean Water, we found that when the northward Mediterranean Water branch weakens in spring and autumn, the westward Mediterranean Water vein strengthens, and vice versa. The maximum net transports of Mediterranean Water across the northern and western sections of the box were estimated at −1.9 ± 0.6 Sv (summer) and −0.8 ± 0.2 Sv (spring), respectively. Within the error bar (0.2 Sv), we found no significant net volume transport of Mediterranean Water across the southern section.

1. Introduction

Progress has been made in understanding ocean dynamics through continuously evolving techniques and methods. Inverse methods were first applied to oceanographic data (in situ temperature and salinity, namely the density field) in the mid-1970s, when it began to be fully recognised that the thermal-wind and conservation equations permitted the estimation of the absolute velocity field as the sum of both the reference level velocity and thermal-wind velocity (Wunsch, 1977, 1978). The inverse box model concept has since been developed, based on both linear and nonlinear procedures (Mercier, 1986; Lux et al., 2001), to provide the best available picture of the global circulation (Ganachaud and Wunsch, 2000). During the 1990s, inverse methods were introduced in the Northeastern Atlantic region to solve the absolute circulation pattern (Arhan et al., 1994; Paillet and Mercier, 1997) and they have since been used widely (Álvarez, 2002; Álvarez et al., 2005; Álvarez and Álvarez-Salgado, 2009; Hernandez-Guerra et al., 2005; Machín et al., 2006a; Lherminier et al., 2007, 2010). In this paper, we focus on the Azores–Gibraltar region; specifically, on a box defined by the World Ocean Atlas 2009 (WOA09) nodes depicted in Fig. 1.

The large-scale surface circulation (0 to ~500 m) in the North-Eastern Atlantic region is dominated by an eastward-zonal basin-scale current, the Azores Current (AC), centred at about

* Corresponding author. Tel.: +34 986 231 930x375.
E-mail addresses: lcarracedo@iim.csic.es (L.I. Carracedo), migil@iim.csic.es (M. Gilcoto), Herle.Mercier@ifremer.fr (H. Mercier), fiz.perez@iim.csic.es (F.F. Pérez).

0079-6611/$ - see front matter © 2014 Elsevier Ltd. All rights reserved.
http://dx.doi.org/10.1016/j.pocean.2013.12.005

List of the acronyms used in the text

Currents

AC Azores Current
ACC Azores Counter Current
CC Canary Current
PC Portugal Current

Water masses

AA Antarctic Intermediate Water (diluted core)
$ENACW_P$ Subpolar East North Atlantic Central Water
$ENACW_T$ Subtropical East North Atlantic Central Water
H Harvey
ISOW Iceland Scotland Overflow Water
LSW Labrador Sea Water
MMW Madeira Mode Water
MOW Mediterranean Outflow Water
MW Mediterranean Water
MW_{nb} Northward Mediterranean Water branch
MW_{wb} Westward Mediterranean Water branch
$NEADW_L$ Lower North East Atlantic Deep Water

Other abbreviations

OC Overturning Circulation
WOA09 World Ocean Atlas 2009

34–35°N (Péliz et al., 2005). After crossing the Mid-Atlantic Ridge between 34 and 36°N (Jia, 2000; Smith and Maltrud, 1999) the AC displays high variability as a result of its meandering (Pingree et al., 1999; Alves et al., 2002; Carracedo et al., 2012). The surface circulation in the Gulf of Cadiz (Fig. 1) has been interpreted as its last meander (Criado-Aldeanueva et al., 2006). Branches of the AC loop gently into the Portugal Current (PC) and further south into the Canary Current (CC) (Barton, 2001). The PC flows equatorwards, at least in the upper layer, and when it reaches Cape St. Vincent, most of the flow turns east (Criado-Aldeanueva et al., 2006) but a small part continues southwards in the surface anti-cyclonic circulation cell to join the CC. The eastward flow forms a surface jet along the Gulf of Cadiz slope/shelf break (Gulf of Cadiz Current) (Péliz et al., 2009), providing 40% of the Atlantic water entering the Mediterranean via the shallow surface layer (Barton, 2001; Criado-Aldeanueva et al., 2006; Péliz et al., 2009). The other

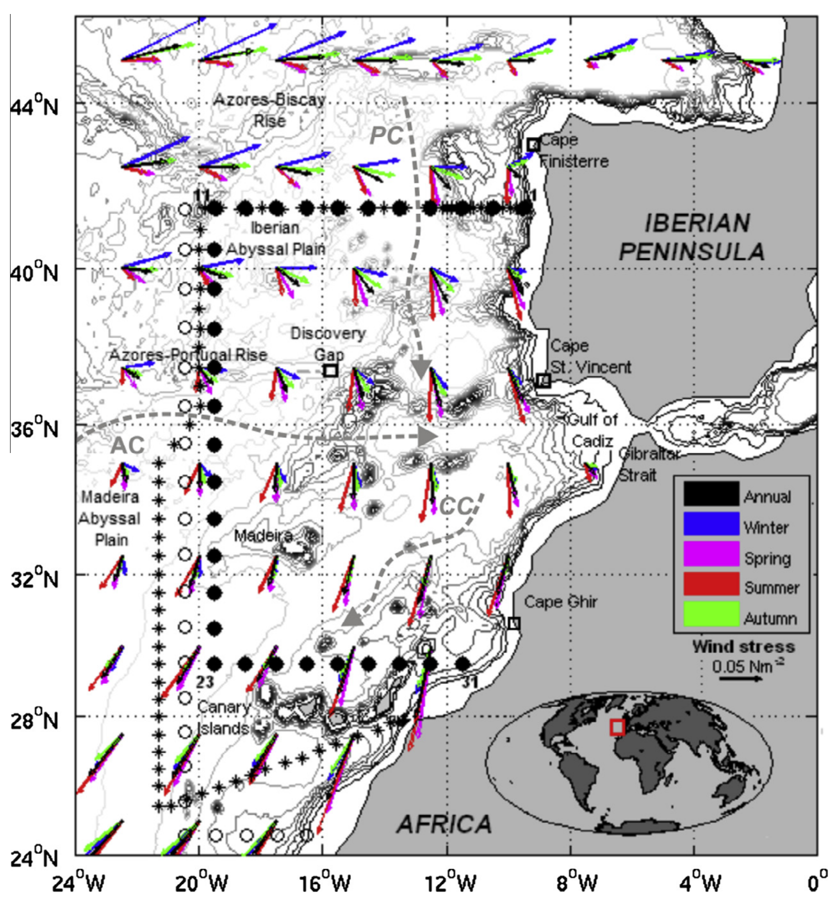

Fig. 1. WOA09 grid defining the box (black dots, labelled as nodes 1–31). The MedBox (Álvarez et al., 2005) and Levitus-MedBox (Slater, 2003) stations appear superimposed (black stars and white dots, respectively). The seasonally-averaged wind field is shown (see colour arrows legend). The figure also includes topographic features cited throughout the text: Azores-Biscay Rise, Azores-Portugal Rise, Discovery Gap, Iberian Abyssal Plain, Madeira Abyssal Plain, Gulf of Cadiz and Gibraltar Strait. Grey dashed lines indicate main surface currents (PC, Portugal Current; AC, Azores Current; CC, Canary Current). (For interpretation of the references to colour in this figure legend, the reader is referred to the web version of this article.)

60% is provided by an offshore Atlantic vein (Péliz et al., 2009), probably fed by the AC.

At intermediate depths (~500 to ~2000 m), in particular at the Mediterranean Water (MW) level (1100–1200 dbar), there is a poleward flow in the Iberian ocean margin (Ambar and Howe, 1979a,b; Mazé et al., 1997; van Aken, 2000b). In this study, we will refer to MW (Ríos et al., 1992; Ambar et al., 1999; Álvarez, 2002; Álvarez et al., 2005; Alves et al., 2011) as the water mass formed in the Gulf of Cadiz (Fig. 1) when the pure Mediterranean outflow water (MOW; Zenk, 1975; Rhein and Hinrichsen, 1993; Baringer and Price, 1997; Huertas et al., 2012) spills over the Gibraltar Sill towards the Gulf of Cadiz, entraining considerable amounts of the overlying central water. By the time this recently ventilated intermediate water mass reaches Cape St. Vincent (Fig. 1) it is neutrally buoyant (at ~1000 dbar) and from there, it spreads through the entire North Atlantic (Arhan et al., 1994; Fusco et al., 2008). The MW flows mainly northwards along the European western margin, parallel to the bathymetry contours to the Porcupine Bank (53°N); however, it also follows a secondary route associated with the westward/south-westward movement of intermediate anticyclonic eddies ("meddies") (Shapiro and Meschanov, 1996; Bower et al., 1995, 1997; van Aken, 2000b). Meddies are formed mainly in the vicinity of Cape St. Vincent (Fig. 1), induced by the sharp bend of the bathymetry and the presence of canyons (Richardson et al., 2000). From here, most of them tend to spread across the southern domain of the region (Arhan et al., 1994; Richardson et al., 2000). At 20°W, authors such as Tsuchiya et al. (1992) observed that the MW core crosses the meridian at approximately 37°N at a depth of about 1000 m; however, this has been related to the Azores Counter Current (ACC) rather than to the westward displacements of meddies.

At the same depth level, the fresher Antarctic Intermediate Water flows northwards along the African ocean margin, reaching latitudes as far as 34°N (Machín and Pelegrí, 2009). Here we will refer to AA as the diluted core of the Antarctic Intermediate Water, according to Álvarez et al. (2005). Below the MW level and south of 48°N, an anti-cyclonic flow of Labrador Sea Water (LSW) brings this water mass, originally transported by the North Atlantic Current, southwards and then westwards past the Azores Islands (Saunders, 1982; Reid, 1994; Paillet and Mercier, 1997). Remnants of the Iceland-Scotland Overflow Water (ISOW) also enter the eastern North Atlantic from a northern source (van Aken, 2000a).

At deeper levels (>2500 m), the Lower North East Atlantic Deep Water ($NEADW_L$) circulates under strong constraint by the topography, forming a cyclonic gyre in the northern part of the eastern basin (Dickson et al., 1985; Arhan et al., 1994; Paillet and Mercier, 1997), between the Discovery Gap and the Azores-Biscay Rise (Fig. 1). The northward-flowing deep water enters a cul-de-sac, due to the topographic morphology, which leads to deep upwelling along the European and Northwest African continental margin (Arhan et al., 1994; van Aken, 2000a).

In this context, the Strait of Gibraltar plays an important role as a topographic feature that effectively separates the eastern boundary ventilation system of the Atlantic Ocean into the northern and southern regions (Barton, 2001), enabling the connection between the MOW and the AC. The overflow is known to have a dynamical impact on the upper-layer circulation in the subtropical eastern North Atlantic (Jia, 2000), generating an area of convergence and downwelling in the Gulf of Cadiz. In a global thermohaline context, the MW contribution to the Atlantic Ocean is significant. Through mixing, the MW raises salinity of the North Atlantic Ocean intermediate domain, which ultimately transfers some thermohaline signature to the lower Meridional Overturning Circulation limb by means of the North Atlantic Deep Water formation (Reid, 1994). Off the Strait of Gibraltar, the Gulf of Cadiz is the transitional sub-basin where the pure MOW experiences strong mixing with the Eastern North Atlantic Central Water. The Gulf is broadly considered the geographic origin of the MW observed in the North Atlantic (van Aken, 2000b; Fusco et al., 2008). This entrainment of Eastern North Atlantic Central Water leads to an overturning circulation in the region.

In this study, we seek a better understanding of the coupling between the horizontal circulation in the region between the Azores Islands and the Gibraltar Strait and the overturning circulation within a climatological framework. We make use of the World Ocean Atlas 2009 (WOA09) data to present a description of the seasonal circulation pattern. To reach this objective, the circulation is derived from a two-dimensional inverse ocean model, which solves the velocity at the reference level problem. Unlike previously published studies in this area, the model exploits climatological and seasonal forcing. The application of a geostrophic inverse model to climatological and seasonal data brings some benefits over the use of synoptic data, because it avoids mesoscale-related uncertainties and problems of synopticity. Thus, this novel approach is a powerful tool with which to attain greater insight into the circulation of the region and to check the consistency of the WOA09 dataset with geostrophic dynamics, as well as to examine the results of using water mass mixing analysis as an additional constraint on the inverse model.

In the following sections we first present the data and the methods for estimating the transports through the box and for solving the water mass mixing (Section 2). Then, we examine and discuss the mean and seasonal circulation patterns in the Azores to Gibraltar Strait region (Section 3). Finally, in Section 4 we present concluding remarks.

2. Data and methodology

2.1. Hydrographic data

Data of in situ temperature, salinity, dissolved oxygen, phosphate, silicate and nitrate come from the WOA09 database (Boyer et al., 2009) (http://www.nodc.noaa.gov/OC5/WOA09/). The data on which this atlas is based come from the World Ocean Database 2009 (http://www.nodc.noaa.gov/OC5/WOD/). WOA09 is a set of objectively analysed (1°-grid resolution) annual, seasonal and monthly climatological fields at 33 standard depth levels for the world's oceans. Temperature and salinity climatologies are the average of five "decadal" climatologies for the following time periods: 1955–1964, 1965–1974, 1975–1984, 1985–1994 and 1995–2006, while oxygen and nutrient climatologies use all available data regardless of the year of observation ("all-data" climatology). The data underwent thorough quality control (Antonov et al., 2010; Locarnini et al., 2010). Values for oxygen and nutrients (NO_3, PO_4 and SiO_4), reported in ml l^{-1} and μmol l^{-1}, respectively, were converted to μmol kg^{-1}. From the WOA09 database, a cruise track-like was constructed by selecting adjacent WOA09 grid nodes that formed a box west of the Gibraltar Strait (referred to as the WOA-Box hereafter) (Fig. 1). In total, 31 WOA09 nodes were selected as hydrographic "stations" (vertical profiles) for later geostrophic, tracer conservation and water mass mixing computation. Hereinafter, the term "node pair" refers to the mid-point between nodes. In addition, when seasonal or monthly heat storage variations were needed as a term for the inverse model heat constraint, all WOA09 nodes within the box were selected for the computation. For further comparison, the WOA-Box boundaries are approximately coincident with the CAIBOX cruise (Carracedo et al., 2012; Fajar et al., 2012). Not all WOA09 variables are available at all depths for all seasons and months. Below 500 m, no seasonal variability is given for nutrient concentrations and it is the same below 1500 m for temperature, salinity and oxygen. Therefore, seasonal and monthly nutrients data were complemented between 500–5500 m (levels 15–33th) with the corresponding annual node profiles and temperature, salinity and oxygen monthly node profiles were complemented between 1500–5500 m (levels 25–33th) with their corresponding seasonal ones.

Other sources of data used in this work were MEDATLAS2002 (http://www.ifremer.fr/medar/), for estimating advective salt fluxes at the Gibraltar Strait and the European Centre for Medium-range Weather Forecast 40-Year Reanalysis (http://www.ecmwf.int/), the Objectively Analyzed air-sea Fluxes for the Global Ocean (http://oaflux.whoi.edu/) and the National Center for Environmental Prediction and Atmospheric Research Global Reanalysis data (http://www.esrl.noaa.gov/) for air-sea volume fluxes. In addition, the mean Ekman-layer transport induced by the wind drag at the sea surface was calculated from the European Centre for Medium-range Weather Forecast 40-Year Reanalysis database (2.5° × 2.5°) (Fig. 1), which was added to the geostrophic transports after having distributed it equally over the first 30-m depth. Annual, seasonal and monthly means were computed from wind data (September 1957 to August 2002).

2.2. The inverse box model

The underlying method behind the inverse model consists of the computation of absolute transports across the WOA-Box boundaries by applying the thermal wind balance to consecutive WOA09 node profiles along the box section and estimating the reference level velocities by use of property conservation equations as constraints (Mercier, 1986; Lux et al., 2001; Lherminier et al., 2007, 2010). Formally, one *a priori* solution – initial guess – for the reference velocities and vertical diffusivities is defined and combined with the constraints (conservation equations) in a generalised nonlinear least squares inverse model through a cost function (J). By the term "conservation equation" we mean a balance between advection and vertical diffusion. The *a priori* solution and the set of constraints are weighted by their associated uncertainty. Finally, the cost function is minimised to estimate the total velocity field across the WOA-Box and we compute the associated uncertainty (the standard error) of the solution.

2.2.1. The unknowns

The unknowns of the inverse model are:

1. The reference level velocity (u_r) normal to the hydrographic lines, for all station pairs (30 pairs).
2. The vertical diffusivities K_v at the interface between layers. The layer limits were selected by σ_3 levels, following Álvarez et al. (2005) and Slater (2003) (hereafter, we will use the notation $\sigma_n = value$ for a potential density of $(1000 + value)$ kg m^{-3} referred to $n \times 1000$ db): 1) from 41.430 (~2500 m) to 41.455 (~2800 m), 2) from 41.455 to 41.475 (~3000 m), 3) from 41.475 to 41.490 (~3200 m), 4) from 41.490 to 41.505 (~2700 m) and 5) from 41.505 to the bottom. A total of five unknown diffusivities are added to the system, which are necessary to compute the diffusive fluxes in the tracer constraints that are written as a balance between the 3D-advection and vertical diffusion.

2.2.2. The reference levels

The reference level for the thermal wind equations is established *a priori*. Usually, one assumes prior zero velocity at the reference level, provided we select an interface between the water masses moving in opposite directions or it belongs to a water mass with a very low motion. Before inversion, however, the reference level velocities do not have to be compatible with the conservation constraints. After inversion, the velocities at the reference level are no longer zero and they are compatible with the various conservation constraints. The initial selection was set at 3200 dbar (~σ_3 = 41.49 kg m^{-3}, ~σ_4 = 45.84 kg m^{-3}) based on previous studies (Saunders, 1982; McCartney, 1992; Arhan et al., 1994; Álvarez, 2002; Álvarez et al., 2005; Álvarez and Álvarez-Salgado, 2009; Lherminier et al., 2007, 2010). From this first guess, we modified the initial reference level under the criterion that the velocity field obtained from just the thermal wind equations must satisfy the circulation patterns in the area. The final selection (Fig. 2 right panel) combined the broadly used σ_3 = 41.49 kg m^{-3} (~3200 dbar) level (node pairs 5–17) with a shallower one at γ^n = 27.922 kg m^{-3} (neutral density level, ~1600 dbar) in the Canary Basin area (node pairs 18–29). The latter is the interface level between intermediate and deep waters (Machín et al., 2006a). For the shallower stations off the Portuguese coast (node pairs 1–4), the selected level was 1800 dbar (as the lower limit for MW influence). Off the African coast, in the vicinity of the Lanzarote Channel (Fig. 1, node pairs 29–30), γ^n = 27.3 kg m^{-3} (~700 dbar) was used, because it is the interface level between central and intermediate waters (Machín et al., 2006a; Fraile-Nuez et al., 2010).

2.2.3. The constraints

The model was forced to conserve volume and salt in the entire water column. Following Álvarez et al. (2005) and Slater (2003), volume, salt and heat were also constrained to remain conserved within individual density layers (σ_3, in kg m^{-3}). In general, the uncertainties for these constraints are selected to be as realistic as possible, taking into consideration the smoothed character of the hydrographic data set.

Furthermore, independent volume fluxes were included as additional constraints (on the northern section and in near-coast areas). Following Lherminier et al. (2010), a transport of −0.8 ± 0.8 Sv was imposed on the northern section (nodes 1–11) from σ_4 = 45.85 kg m^{-3} to the bottom. This transport agrees with McCartney et al. (1991) estimation of 0.83 Sv for θ < 2.5 °C at 36°N between 16 and 19°W. For the eastern boundary of the northern section (nodes 1–3) −1 ± 1 Sv from σ_2 = 36.94 kg m^{-3} to the bottom was set following Lherminier et al. (2010). On the southern section, seasonally varying climatological values from direct estimates for the Eastern North Atlantic Central Water and AA in the Lanzarote passage area (Fraile-Nuez et al., 2010) were included.

Finally, the deep water mass conservation was reinforced by adding a new constraint, which involved an extended Optimum Multiparameter (eOMP) solution. The eOMP method (Karstensen and Tomczak, 1998) consists of quantifying the fractions of a specific set of source water masses that may compose each sampled water parcel. This method accounts for the non-conservative character of some of the parameters (O_2, NO_3, and PO_4) by taking into consideration the biogeochemical processes; this is done by means of Redfield ratios. The eOMP used here (for further details see Carracedo et al., 2012; Pardo et al., 2012;) includes a combination of both classical (θ, S, SiO_4, NO, PO) and extended (θ, S, SiO_4, O_2^o, NO_3^o, PO_4^o – the last three being the preformed values for these variables) OMP. The variables are weighted in function of their associated uncertainty. Also, the resolution algorithm of the method implements an iterative procedure to successively reduce the residuals on the nutrient balances (Pardo et al., 2012). As a constraint to the minimisation process, mass conservation must be rigorously satisfied and the contribution of each source water mass must be positive.

The resulting water mass contribution matrix (with values in the range 0–1), gives the amount of a certain water mass implicated in the mixing process. With this new "weighting" matrix, one can constrain a specific water mass transport without assuming that one water mass is purely delimited by density boundaries;

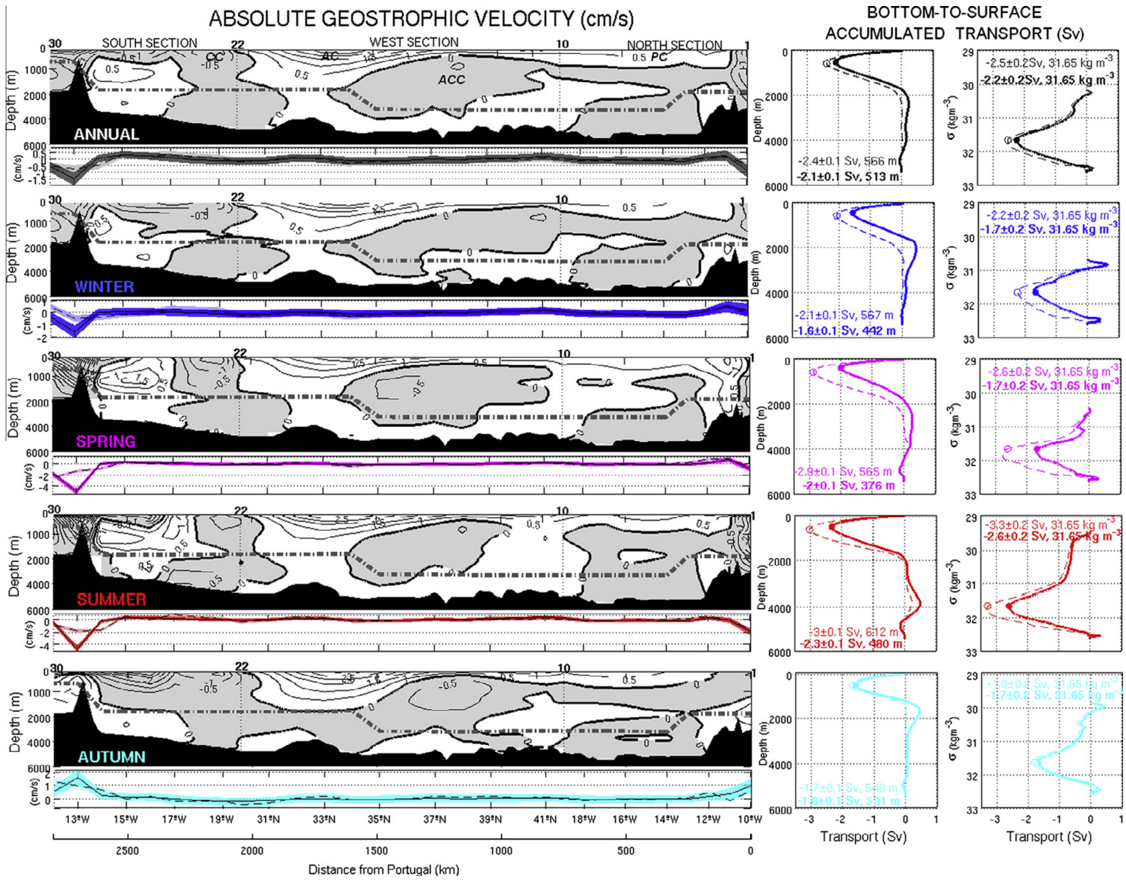

Fig. 2. (Left) Contour plots of absolute geostrophic currents for the WOA-Box (T_1) (inside box view is set up). Grey shaded area indicates (negative) outgoing velocities and white shaded area (positive) incoming velocities. Initial reference level is also plotted (dashed-point grey line). Under-contour charts present reference level velocities after inversion (black straight/dashed lines for T_1/T_0, respectively) with their error interval (shadings). (Right) Charts of accumulated transports (Sv) in depth (left) and density levels (right). Again, straight and dashed lines mean T_1 and T_0, respectively.

thus, providing an additional constraint to the inverse model. Here, the model was constrained to conserve the sum of deep waters: LSW + ISOW + NEADW$_L$. Previously addressed by studies such as that by Álvarez et al. (2005), this methodology leads to a more detailed constraint on deep water transports, providing favourable feedback to the inverse model. To be consistent with the volume errors by layers, an uncertainty of ±0.2 Sv was finally established.

2.2.4. Final model set-up

Two approaches were undertaken in this study. The first, labelled as Test 0 (T_0), focused on reproducing the model configuration used by Slater (2003) (hereinafter referred to as S03), who used Levitus climatology data in a similar box. This approach departs from the "simplest" reference level configuration. Only constraints of volume, heat and salt conservation in deep layers (>~2500 m), plus surface-to-bottom volume and salt conservation, were included. On this basis, the choice of uncertainty amplitude let us force a solution equivalent to that of S03 where the volume was constrained to zero, which resulted in a net salt flux across the boundaries of the WOA-Box. Therefore, in T_0, the zero net volume transport uncertainty was assigned a value of ±0.1 Sv. The salt constraint was defined as the net salt transport obtained by S03's annual/seasonal solutions with a 10% uncertainty (Ganachaud et al., 2000, without their factor of 4). As such, a small volume conservation uncertainty could push the limits of what is physically consistent; therefore, we have decided to keep this solution just for the discussion.

The second approach, our best solution, called Test 1 (T_1), changes the way in which the surface-to-bottom volume and salt conservation assumptions are settled. It is more consistent physically in that the excess of evaporation (E) over precipitation (P) and runoff (R) in the region of the WOA-Box and Mediterranean Sea is compensated by a net water transport into the box and not through a net salt flux. In terms of the model, this is applied by strictly conserving salt (0 ± 10^6 kg s^{-1}) and by requiring the volume to account for the E–P–R term with an uncertainty of ±1 Sv. Moreover, this configuration uses a different *a priori* reference level, chosen after a sensitivity test was applied, which includes the additional independent volume constraints taken from the bibliography. Table 1 summarises these two configurations.

2.2.4.1. The a priori solution. Ultimately, lateral continuity of the velocity at the reference level after inversion depends on the uncertainty we assume *a priori* for each reference level. For both tests, the *a priori* error for the reference level velocities was selected to be 0.3 cm/s. As S03's solution did not include uncertainties in the computations, 0.3 cm/s is a value that comprises the highest velocity at the reference level obtained with their solution. This value is also consistent with the weak circulation implied by the use of climatology (Fig. 2). In the case of T_1, the velocity errors *a priori* in coastal pairs were doubled to 0.6 cm/s to account for higher uncertainty in these areas. The velocities at the reference level and their errors after inversion (for T_0 and T_1) are shown in Fig. 2.

The vertical diffusivity term K_v was set *a priori* to a generalised value of $10^{-4} \pm 10^{-4}$ m^2 s^{-1} for all the interfaces between the layers (Mazé et al., 1997; Polzin et al., 1997; Lux et al., 2001) and for both

Table 1
(a) Summary of the annual constraints, (b) seasonal change in volume and salt constraints (T_1).

Constraint	Test	Value	Horizontal domain vertical domain	After inversion
Surface-to-bottom volume conservation (Sv)	T_0, T_1	0 ± 0.1, 0.071 ± 1	Entire box Entire water column	−0.04 ± 0.1, 0.01 ± 1
Surface-to-bottom salt conservation ($\times 10^9$ kg/s)	T_0, T_1	−1.55 ± 0.2, 0 ± 10^{-3}	Entire box Entire water column	−1.55 ± 0.2, 0 ± 10^{-3}
Volume, salt and heat conservation by deep layers	T_0, T_1	0 ± $K_v A \delta\Phi/\delta z$	Entire box σ_3 > 41.430 kg/m^3 (∼2600 m to bottom)	−0.01 to 0, 0.02–0.08
Surface-to-bottom LSW + ISOW + NEADW$_L$ conservation (Sv)	T_1	0 ± 0.2	Entire box See WM distribution, Fig. 5a	−0.39 ± 0.2
(1) NEADW$_L$-IAP transport (Sv)	T_1	−0.8 ± 0.8	North section (St pairs 1–10) σ_4 > 45.85 kg/m^3 (∼3700 m to bottom)	−0.56 ± 0.8
(2) SADCP-based transport (Lherminier et al., 2010) (Sv)	T_1	−1 ± 2	Eastern Boundary Current (St pairs 1–2) σ_2 > 36.94 kg/m^3 (∼2000 m to bottom)	−0.08 ± 2
(3) Central water off Africa coast transport (Fraile-Nuez et al., 2010) (Sv)	T_1	−0.81 ± 0.5	Lanzarote Passage (St pairs 29–30) Surface to γ = 27.3 kg/m^3 (0–600 m)	−1.83 ± 0.5
(4) AA off Africa coast transport (Fraile-Nuez et al., 2010) (Sv)	T_1	0.09 ± 0.5	Lanzarote Passage (St pair 30) γ = 27.3 kg/m^3 to γ = 27.7 kg/m^3 (600–1100 m)	−0.21 ± 0.5

	Volume (Sv)				Salt ($\times 10^9$ kg/m^3)	
	Air-sea flux WOA-Box (E–P–R) (ERA40)	Air-sea flux MedSea (E–P–R) (ERA40)	Volume flux constraint		Salt flux constraint	
Winter (1–3)	−0.024	−0.026	0.050	±1	0	±0.001
Spring (4–6)	−0.032	−0.019	0.051	±1	0	±0.001
Summer (7–9)	−0.040	−0.051	0.091	±1	0	±0.001
Autumn (10–12)	−0.042	−0.051	0.093	±1	0	±0.001
Annual mean	−0.034	−0.034	0.071	±1	0	±0.001

tests. After inversion, we obtained higher values (ranging between 1.5–2.0 $\times 10^4$ m^2 s^{-1}) than the *a priori* ones as could be expected for a box including strong interactions between currents and topography (Polzin et al., 1997).

In summary, a total of 35 unknowns, velocities at the reference level for 30 nodes pairs, 5 diffusion coefficients for the interfaces between the 6 defined layers and 17 (T_0) or 22 (T_1) constraints comprise the system (Table 1). Therefore, the cost function (J) could be expressed as:

$$J = \sum_{ip=1}^{N_{pair}} \left(\frac{u_r^{ip} - u_{r_0}^{ip}}{\sigma_{u_{r_0}}^{ip}} \right)^2 + \sum_{ii=1}^{N_{interface}} \left(\frac{Kv^{ii} - Kv_0^{ii}}{\sigma_{Kv_0}^{ii}} \right)^2 + \left(\frac{T^{sb} - T_0^{sb}}{\sigma_{T_0}^{sb}} \right)^2 + \sum_{ip=1}^{N_{pair}} \int_{z_l}^{z_u} \left(\frac{T^{layer} - T_0^{layer}}{\sigma_{T_0}^{layer}} \right)^2 + \sum_{iocon=1}^{N_{other\_constraintes}} \sum_{ip=L}^{M} \int_{z_{inf}}^{z_{sup}} \left(\frac{T^{ocon} - T_0^{ocon}}{\sigma_{T_0}^{ocon}} \right) \quad (1)$$

Subscript 0 means *a priori* established values and σ indicates the uncertainty on these *a priori* values, u_r^{ip} is the reference level velocity at node pair *ip* after inversion, Kv^{ii} is the vertical diffusion coefficient at interface *ii* after inversion, T^{sb} represents the surface-to-bottom (*sb*) volume, salt and heat conservation constraints after inversion, T^{layer} are the conservation constraints (volume, salt and heat) by layers and are the specific transports included as additional constraints (other constraints, *ocon*, where deep water masses conservation in also included). The transports shown hereinafter will be taken as positive entering the box.

3. Results and discussion

One important consideration when we work with climatological data is the smoothed character of the thermohaline gradients. This impacts the results directly in terms of weaker geostrophic velocities and a greater reduction of mesoscale variability than would be found in a synoptic cruise; however, the impact is partially compensated, in terms of volume transport, by the widening of the currents. Of particular concern with these data is the transport of salt, especially in this area of the ocean. The dispersion of MW in the Atlantic Ocean is known to be reinforced by the action of mesoscale meddies detaching from the Mediterranean Undercurrent (Ambar et al., 1999). Lateral intrusive mixing at the eddy boundaries and to a lesser extent, double-diffusive mixing, are responsible for most of their salt and heat loss (Armi et al., 1989). It is worth noting that most of the data used to derive the WOA09 dataset were acquired after the 1970s, when quality control algorithms were adapted to cope with the existence of the meddies; therefore, they are expected to have been properly included in the climatology (in averaged form). The reduction of the mesoscale signal in the climatological data set means that the horizontal salt fluxes at mid-depths are underestimated, which means that the present results may be considered as lower bound estimations.

In the following, we show the main results for our best model configuration (T_1) in terms of the main surface/subsurface currents; the error bars account for the differences with the T_0 solution. Only the significant differences between the two models will be highlighted in the text. Furthermore, note that Section 3.1.1 will be presented as a validation section as well, providing robustness to the results.

3.1. Velocity field and volume transports

3.1.1. Surface–subsurface horizontal circulation

The absolute velocity fields that results from the annual and seasonal inversions (test T_1) are shown in Fig. 2. At intermediate and upper levels (surface to ∼2000 m), the main currents represented by the climatological data are AC, ACC, PC and CC (see labels over top contour at Fig. 2). The lower latitudes of the western section are occupied by the inflowing AC. Below the AC (approximately at 1000 m) and further north, there is a westward current that can be directly associated to the ACC (Onken, 1992). On the northern section, the southward-flowing PC and the predominantly winter and autumn Iberian Poleward Current (Haynes and Barton, 1990) may be identified. Finally, flowing out of the WOA-Box across the southern section, the CC may be identified.

3.1.1.1. Azores Current. The AC appears, between 1500 and 2000 km from node 1, to be confined mostly to the upper 1000–1500 dbar. For computing the AC transport, we prepared a grid with a resolution of 1 dbar × 0.01° (latitude degrees). Then, the eastward transports higher than 0.001 Sv between 30–37°N, the range in which the AC was identified graphically, were integrated for annual, seasonal and monthly climatologies (see monthly AC variability in Fig. 3a). The AC transport is known to range from 9 to 12 Sv between 30–40°W and reduces to around 3–4 Sv closer to the African coast (New et al., 2001). In this work, the annual AC transport was quantified as 6.5 ± 0.8 Sv at 19.5°W, which is close to that obtained by Pingree et al. (1999) from the WOA94 data base (6.7 Sv, with reference level of 2000 dbar) and not far from other estimates derived from hydrographic cruises (9.3 ± 2.6 Sv at 20°W (Carracedo et al., 2012), 6.8–7 Sv at 21–19°W (Alves et al., 2002)). Its broadened width prevents us establishing a precise latitudinal position; however, if we compute a value for the AC core width, that is, the area of velocities higher than 2 cm/s, we find it is narrowest in spring and widest in autumn. In addition, in spring, the AC velocity maximum is the lowest (2.7 cm/s), the current narrows (~240 km) and its maximum depth is minimal (~790 m); therefore, the net AC transport is lower (5.3 ± 0.8 Sv), particularly in June (2.5 ± 0.4 Sv). From this minimum transport in spring, it increases gradually during summer, reaching a maximum in autumn when, regardless of the test, the seasonal AC velocity maximum is higher (~3.2 cm/s) and the current is deeper (~1100 m) and broader (~400 km), resulting in higher transport (7.3 ± 0.8 Sv), which is in agreement with Klein and Siedler (1989). On a monthly basis, we find a relative maximum in September (9.0 ± 0.9 Sv) but an absolute maximum in January (10.2 ± 0.9 Sv) (Fig. 3a). Although the AC appears broader than it really is, it exhibits a coherent seasonal variability.

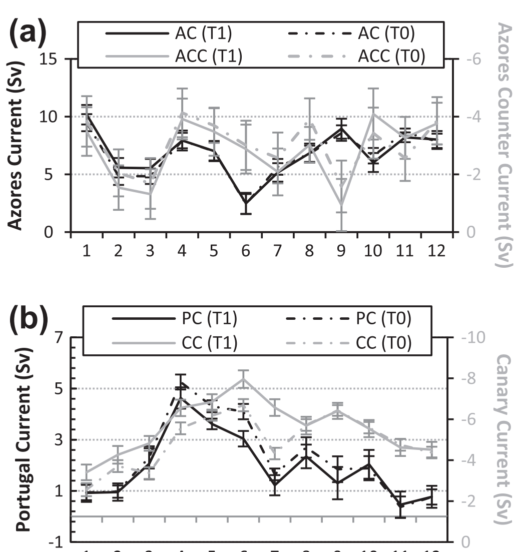

Fig. 3. Climatological monthly time series (January to December) of the main currents of the WOA-Box surface-subsurface circulation, (a) Azores Current (AC) and Azores Counter Current (ACC) and (b) Portugal Current (PC) and Canary Current (CC), under different constraints (T_0 and T_1, see text).

Following previous studies (Onken, 1992; Paillet and Mercier, 1997; Alves et al., 2002; Pérez et al., 2003; Kida et al., 2008; Carracedo et al., 2012) and despite the controversy over its permanent existence (Alves et al., 2002), the subsurface westward stream north of the AC, is associated with the ACC (Onken, 1992). An equivalent procedure, such as that used for estimating the AC was followed for the ACC, computed in this case as the integrated outflowing transport in the first 1800 dbar between 36 and 40°N. This current, irrespective of the test (T_0 or T_1), appears intensified in spring (−3.1 ± 0.9 Sv) and autumn (−3.6 ± 0.8 Sv) with lower transport in summer (−1.9 ± 0.7 Sv) and winter (−1.7 ± 0.8 Sv). In autumn, the ACC is most intense and easiest to identify as a westward jet. Previous estimations of ACC transport by Alves et al. (2002) were in the range 2–5 Sv. They gave a specific transport for a July hydrographic survey of 2.6 Sv at 21°W.

Although the monthly variability of the AC and ACC does not seem obviously related (Fig. 3a), a ratio (not shown) between both flows was estimated by season. In spring and autumn, the AC transport is twice that of the ACC. On the other hand, during winter and summer, the AC transport is four times higher than that of the ACC. The transport ratio variability is higher in summer (1.4 std), and lower in autumn (0.7 std). The higher variability of the AC/ACC ratio in summer could be understood as the enhanced meandering character of the AC during this season, as identified by Klein and Siedler (1989). Again, comparing with the work of Alves et al. (2002) at 21°W, their computed AC/ACC transports led to a ratio of 2.6 (July). Comas-Rodríguez et al. (2011) gave an AC transport in October 2009 of 13.9 Sv and an ACC of 5.5 Sv (24.5°W), resulting in an AC/ACC ratio of 2.5. The significance of this ratio on the seasonal scale needs further investigation. Based on the present study, we suggest that the AC transports twice as much as the ACC in spring (slightly more) and autumn (slightly less), while ratios of higher-than-two in these surface circulations occur in summer and winter.

3.1.1.2. Portugal Current. The PC transport was estimated as the integrated inflowing transport in the first 1100 dbar through the northern section. This current exhibits seasonal variability with a maximum in spring (3.5 ± 0.6 Sv, seasonal mean), reaching a maximum transport of 5.20 ± 0.3 Sv in April (monthly mean, Fig. 3b). This maximum may be related to the upwelling regime that reinforces the southward coastal branch of this current (Barton, 1998, 2001; Navarro-Pérez and Barton, 2001). From spring to autumn/winter, the PC transport weakens to reach minimum values of 0.81 ± 0.2/0.99 ± 0.3 Sv. Stramma and Siedler (1988) estimated a mean autumn value (west of 35°W for the upper 200 m) of 1.4 Sv and a mean annual value (between 20°W and the coast) of 2 Sv. This annual mean is slightly higher but comparable with the annual mean computed in this case (1.5 ± 0.4 Sv).

The presence of a winter Iberian Poleward Current at the central water level off the Iberian coast has been reported widely (Haynes and Barton, 1990; Mazé et al., 1997; Barton, 1998, 2001; van Aken, 2000b; Pérez et al., 2001; Álvarez-Salgado et al., 2003; Péliz et al., 2003). This northward flow forms part of the PC system and it reduces the net PC southward transport in autumn/winter. With our T_1 solution, we computed the Iberian Poleward Current transport as the northward flowing waters above 300 m with salinities higher than 35.8, following Pérez et al.'s (2001). For autumn and winter, a transport of 0.2 ± 0.1 Sv with a maximum in January of 1 ± 0.1 Sv were found, while it was absent between the months of May to August. For a similar location, Frouin et al. (1990) estimated a geostrophic transport (referenced at 300 dbar) for this current of 0.5–0.7 Sv.

3.1.1.3. Canary Current. The CC transport was computed as the integrated outflowing transport above 600 dbar on the southern section and the southern part of the western section, south of 32°N. An annual mean transport of −4.0 ± 0.4 Sv was obtained with a minimum in January (−3.4 ± 0.4 Sv) and a maximum in June (−8.0 ± 0.4 Sv) (Fig. 3b). Using an inverse model, Paillet and Mercier (1997) estimated a mean spring-summer CC transport of about 6 Sv, which is in agreement with our spring-summer estimation (6.0 ± 0.4 Sv).

The CC is stronger in summer near the African coast, east of the Canary Islands, whereas in winter, its maximum migrates to the west of the Canaries (Barton, 1998; Navarro-Pérez and Barton, 2001; Machín et al., 2006a). Our results indicate that the lowest CC transport near the shore (15°W to 12°W) of 0.7/1.6 Sv occurs in autumn/winter, as was also found by Machín et al. (2006a), who estimated a minimum net southward flow for an equivalent width (from surface to ∼700 m) of 0.9/1.5 Sv (their Fig. 20b and c). They also reported a strong cyclonic eddy recirculation west of Lanzarote and Fuerteventura in spring and an autumn westward migration of the CC branch, as seen in the WOA09 data (see Fig. 2 left panel, spring and autumn). This recirculation allows a northward volume flux (surface to 700 m) between the Canary Islands and the African coast estimated (from surface to ∼700 m) at 0.8 Sv, as compared with 1.8 ± 0.1 Sv (Machín et al., 2006a). As has been seen, both the PC and CC exhibit similar seasonality with a positive significant correlation (95% confidence interval) of 66% (Table 2).

In general terms, all transports given by our estimations from seasonal climatological inversions agree reasonably well with those seasonal quasi-synoptic cruise-derived transports in the same area. This validates the idea that climatological data can be used to establish a seasonal characterisation (lower-bound estimations) of the principal geostrophic currents.

3.1.2. Vertical circulation structure

The main vertical structure of the circulation across the limits of the WOA-Box consists of an upper inflowing layer above ∼500 m (Fig. 2 right panel) and an intermediate outflowing layer between ∼500 and ∼2000 m. Generally, bottom waters present weak flow (<0.5 cm/s), except in the Canary Basin (12–19.5°W), where an enhanced recirculation of deep waters in summer can be discerned (Fig. 2 left panel, summer).

The vertically accumulated transports allow us to quantify the overturning circulation in the box (OC, hereinafter). OC can be defined as the magnitude of the upper inflow into the box (Slater, 2003; Álvarez et al., 2005); however, here, we calculate it by accumulating the transport (by pressure and density anomaly levels) from bottom to surface, because the non-zero net transport would be expected to be mainly a consequence of the surface large-scale circulation through the limits of the box.

If we compare the OC values obtained by the two integration methods (pressure and density), they differ by 0.4 Sv as a maximum. As the OC is a measure of the conversion of lighter waters into denser waters as they entrain in deeper levels, as well as water masses spread by isopycnal levels, it seems to be more reliable to consider OC transport in terms of density layers. The vertical accumulation of the net transport in the box by density layers (Fig. 2 right panel, right chart) allows us to separate the OC in its upper inflowing and lower outflowing limbs by the σ_1 = 31.65 kg m^{-3} isopycnal layer (hereinafter σ_{OC} will be used to designate the isopycnal of the OC maximum). The annual mean magnitude of the OC into the box is 2.2 ± 0.2 Sv (slightly higher when considering T_0, 2.5 ± 0.2). In summer, we find the highest OC for both tests (2.6 ± 0.2 and 3.3 ± 0.2 Sv); nevertheless, the minimum OC differs between the tests. It occurs in autumn (1.8 ± 0.2 Sv) in the case of T_0, whereas T_1, the same OC is found for the other three seasons (1.7 ± 0.2 Sv).

Table 2
Correlation between the different overturning system components (linear regressions shown for T_1). R^2 is the determination coefficient at the 95% confidence interval (T_1(T_0)).

	LeastSquareFitting	R^2
Portugal Current vs. Canary Current[a]	$y = 0.84x + 3.97$	0.66 (0.60)
Overturning Circulation vs. Central Water	$y = 0.97x + 0.70$	0.94 (0.97)
Overturning Circulation vs. Mediterranean Water	$y = 0.66x - 0.30$	0.88 (0.70)
Mediterranean Water vs. Central Water	$y = 0.71x + 0.62$	0.90 (0.69)

[a] The component is ahead one month with respect to the other.

3.2. Water masses circulation

The potential temperature/salinity (θ/S) diagrams in Fig. 4 allow us to describe spatially the annual mean hydrography. We depict the transport field (T_0 vs. T_1 velocity field solution) in the θ/S diagrams as coloured contours giving us a first general perspective of the dynamics in the WOA-Box. From north to south, surface waters (above σ_1 = 31.8 kg m^{-3} isopycnal, central water layer) increase their temperature and salinity whereas the salinity of intermediate waters (between σ_1 = 31.8 to σ_1 = 32.25 kg m^{-3}, MW layer) diminishes. In the northern section, the highest salinity (36.192) is found at the MW level. The highest surface thermohaline variability occurs along the western section because of the meridional gradient (frontal zone area). In the climatological annual mean, the Azores Front (Pérez et al., 2003) has been located between 34–35°N (between node pairs 17 and 18), associated with the maximum AC velocity (34°N).

The general circulation pattern that can be deduced is that southern-origin surface waters (those above σ_1 = 31.8 kg m^{-3}), Madeira Mode Water (MMW, Siedler et al., 1987) and Subtropical Eastern North Atlantic Central Water (ENACW$_T$, Ríos et al., 1992), recirculate clockwise all year round, entering the box through the western section (Fig. 4c and d) and exiting through the southern section (Fig. 4e and f). This result is independent of the test and therefore, the upper anticyclonic circulation pattern is well determined. The isopycnal level that separates the upper and lower limbs of the OC (σ_1 = 31.65 kg m^{-3}) is above the isopycnal interface between the central water and MW layers (σ_1 = 31.8 kg m^{-3}). Therefore not all the OC into the WOA-Box can be assigned to water mass transformation. Part of the inflowing central water downwells inside the box, leading to a recirculation of the lower central water bound (between 31.65 and 31.8 kg m^{-3}) out of the box.

At intermediate levels (between the isopycnals of σ_1 = 31.8 and σ_1 = 32.25 kg m^{-3}), MW leaves the box following two principal paths: one through the northern section (Fig. 4a and b; northern MW branch, MW$_{nb}$) and the other through the western section (Fig. 4c and d; westward MW branch, MW$_{wb}$). The MW$_{wb}$ recirculates and therefore, more pure MW leaves the box but more mixed/diluted MW re-enters.

Regarding the bottom water circulation, there is a marked pattern with deep water coming through the western section and leaving the region through the northern section (Dickson et al., 1985; Álvarez et al., 2005). Firstly, for T_1, deep waters enter through the western section and leave the box mainly across the northern section. Conversely, both western and southern sections present deep water recirculation in the case of T_0. For a quantitative description of these water mass transports we will use the eOMP solution in the next section.

3.2.1. Water masses contribution

The annual mean spatial water mass distribution based on the eOMP run is shown in Fig. 5a. MMW is present along the

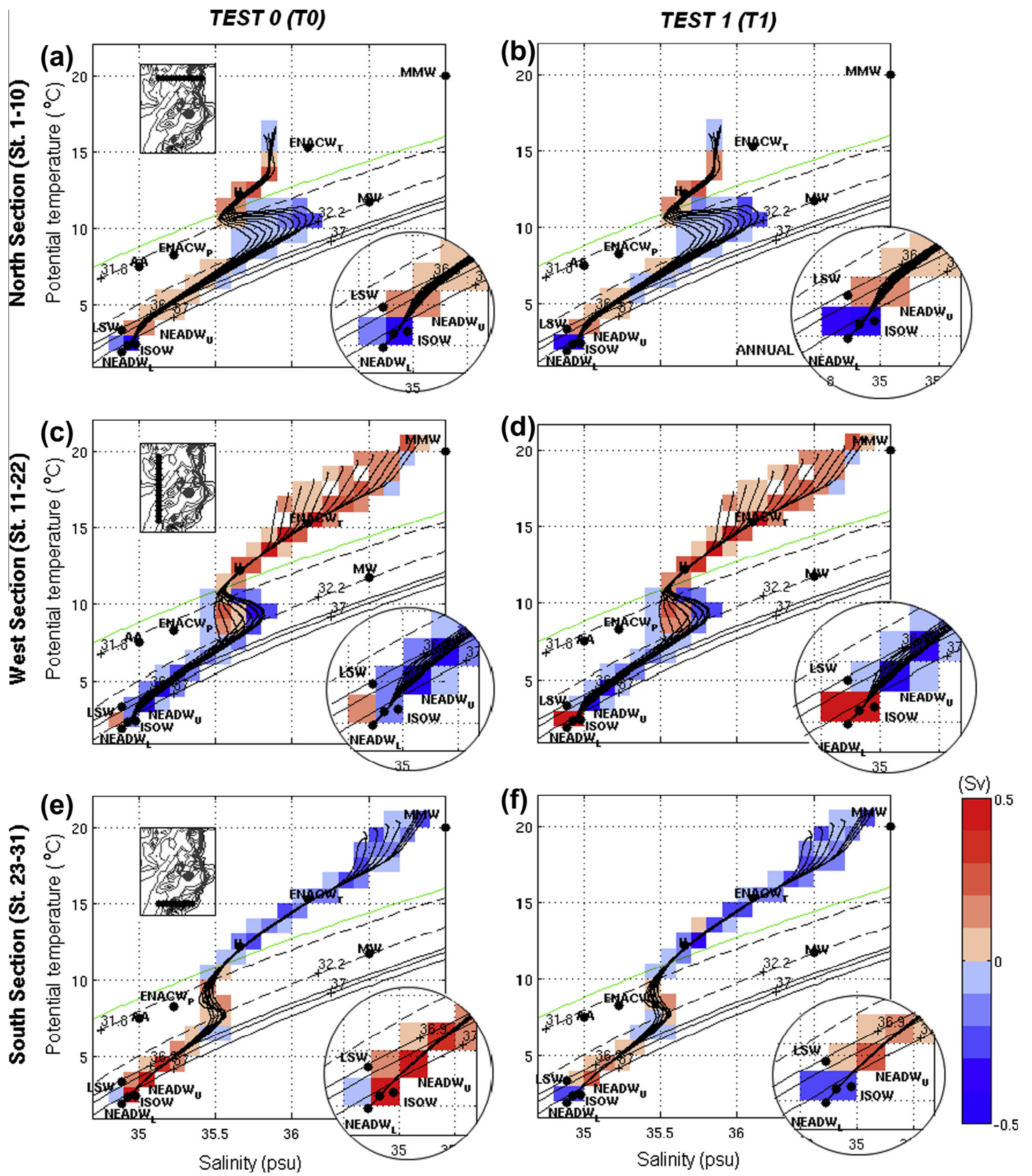

Fig. 4. Potential temperature (surface reference level) vs. salinity diagrams for annual mean (T_0 left column, T_1 right column) and for Northern, Western and Southern sections (in rows from top to bottom). Dashed isolines correspond to potential density anomaly at 1000-m reference level (σ_1 = 31.8 and 32.25) and black thin isolines correspond to potential density anomaly at 2000-m reference level (σ_2 = 36.89, 36.95 and 37.05), all in kg m^{-3}. These isopycnals delimit the water masses into six regions: ENACW layer (surface to σ_1 = 31.8), MW layer (σ_1 = 31.8 to σ_1 = 32.25), MW-LSW layer (σ_1 = 32.25 to σ_2 = 36.89), LSW layer (σ_2 = 36.89 to σ_2 = 36.95), deep mixed layer (σ_2 = 36.95 to σ_2 = 37.05) and NEADW layer (σ_2 = 37.05 to bottom). Additionally, the isopycnal where the OC has been defined is also included (σ_{OC} = 31.65 kg m^{-3}, green line). Black dots mark the position of the source water masses. Filled colour contours of transports (Sv) are given by bins of 0.5 °C and 0.1 psu, positive (red) entering the WOA-Box.

southwestern corner of the WOA-Box, covering the upper 250 dbar of the water column. Following at depth, the ENACW$_T$ reaches its maximum contribution near 250 dbar on the southern section and its range in depth diminishes towards the north, where it is found at the surface. In the range 100–700 dbar, H (Ríos et al., 1992, in honour of Harvey) marks the transition from subtropical (shallower) to subpolar (deeper) central waters. Its higher northward contribution marks the location where the frontal area between both varieties occurs. The main core of the colder subpolar variety of the Eastern North Atlantic Central Water (ENACW$_P$, Ríos et al., 1992) lies close to 900 dbar, being eroded by the spread of the MW. The AA core is found just below 1000 dbar, in the southern and southwestern parts of the box with a maximum contribution of 45% in the vicinity of the Canary Archipelago. The MW core is located just above 1000 dbar with its highest contribution (up to 73%) on the northern section, i.e., it suffers a 27% dilution from its formation in the Gulf of Cadiz. The main water mass cores are coincident with the western and northern branches of the MW

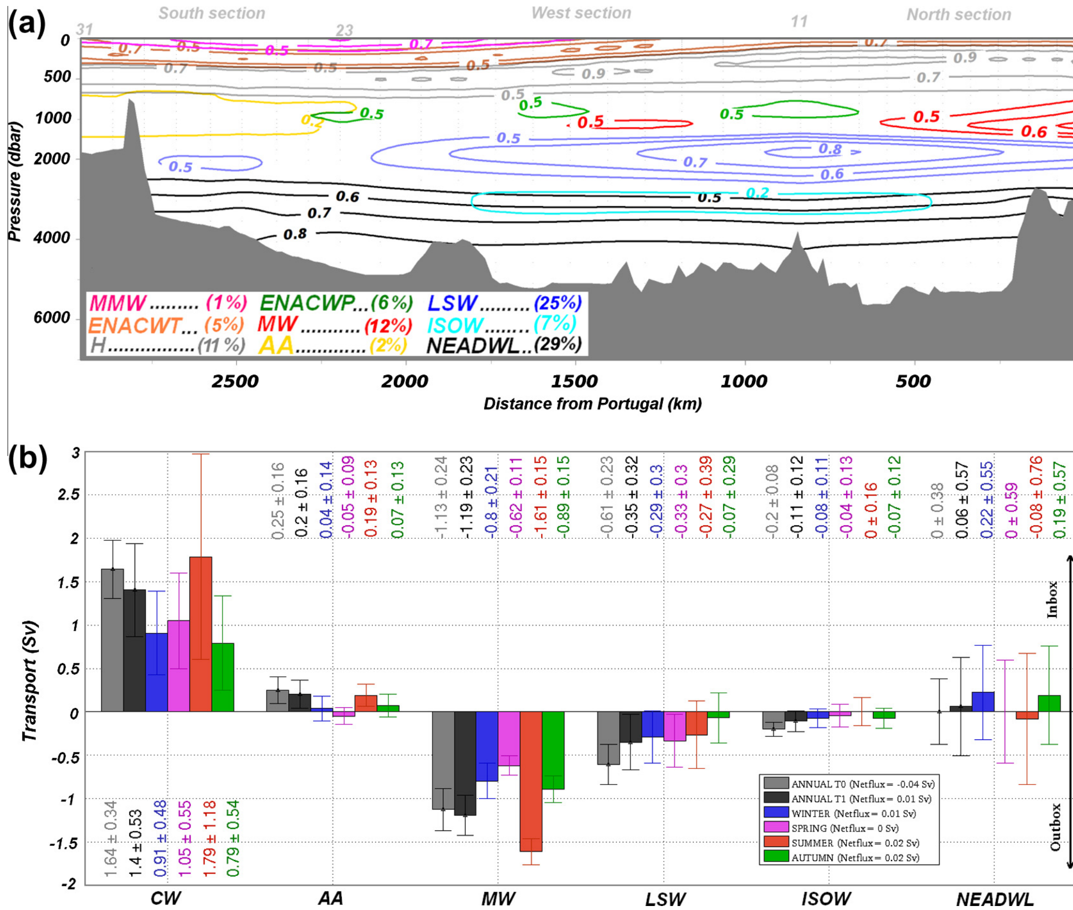

Fig. 5. eOMP results: (a) water masses spatial distribution for annual mean. Contour lines are plotted for contributions >50%, except for the AA and ISOW, whose contour lines represent a contribution >20%. Note that vertical scale has been amplified in the first 1000 dbar for clarity. Figures in parentheses in the legend are percentages of occupied area by water mass (100% represents the area for the entire section). (b) Bar diagram for annual, seasonal and monthly water mass net transport in the WOA-Box. Error bars are also shown for each period (errors given by inverse model).

tongue. The westward branch is connected to the ACC, as we will see in following sections. The highest contribution of LSW (80%) is found in the northwestern corner of the box. Another core appears in the southern section, possibly related to some northeastern recirculation of the LSW, as we will discuss later. Finally, $NEADW_L$ occupies the entire deep water column below 2000 dbar with a contribution above 70%.

In volumetric terms, the percentage of the water column with respect to the entire section area occupied by each water mass remains quite stable despite the season of the year (seasonal values not shown, annual values in Fig. 5a).

3.2.2. Coupling inverse box model – eOMP solution

After solving the water mass contributions with the eOMP, we estimate water mass transports by multiplying the percentages field by the absolute volume transports field. In this way, we evaluate whether it is possible to obtain consistent results by combining eOMP with the inverse model solution (in terms of climatological WOA09 data). To do this requires both the interpolation of the vertical standard-level percentages matrix to a depth resolution of 1 dbar and a horizontal averaging of every pair of nodes; thus, matching the volume transport field.

In Fig. 5b, the seasonal net water mass transports are shown for test T_1. Test T_0 net transports are only shown for annual means (see grey bars). MW is always leaving the box with maximum net outflowing transport in summer (-1.6 ± 0.2 Sv) and the minimum in spring (-0.6 ± 0.1 Sv). Central water maximum net inflowing transport also occurs in summer (1.8 ± 1.2 Sv). The total transport of AA across the section is nearly zero. However, the net positive transport found in summer and in the annual mean (0.2 ± 0.2 Sv), could support the hypothesis that the diluted form of AA contributes to MW formation in the region of the Gulf of Cadiz (Louarn and Morin, 2011). Major discrepancies between T_0 and T_1 come from the LSW net transport. As we know, LSW cannot be formed inside the WOA-Box; thus, a negative net transport for this water mass could be a sign that the T_0 approach is less appropriate.

To evaluate further the seasonal/monthly upper circulation of the WOA-Box, we estimated the relative contribution of each water mass transport to the total transport for each current delimited and described in section 3.1.1 (AC, ACC, PC and CC). The AC transports mainly central water (~90%) with ~50% comprised of the subtropical variety inside the box. The maximum contribution of $ENACW_T$ to AC occurs in spring (57%), whereas the proportion of MMW increases in summer (24%). The MW recirculates into the AC with a maximum 6% of the total AC transport in the autumn-winter period. The ACC exports central water (~40%), in this case mainly the subpolar variety (maximum contribution in autumn, 46%); an important contribution of 25% is MW and LSW (~20%), which also recirculates out of the box. Both PC and CC currents transport mainly central water (>95%). During spring, the contribution of $ENACW_P$ to the PC exceeds that of $ENACW_T$, whereas during the autumn-winter period, this proportion reverses. In addition, the PC has little presence of MW (2% the annual mean and up to 8% in spring). On the other hand, ~60% of the CC transport is $ENACW_T$, which recirculates from the AC. The MMW contribution increases in autumn at the expense of the drop in the $ENACW_T$ contribution.

3.2.3. The overturning circulation system in the WOA-Box

As shown in Section 3.1.2, the annual mean for the OC into the box was 2.2 ± 0.1 Sv with a maximum OC in summer, 2.6 ± 0.1 Sv, and a minimum in winter, 1.7 ± 0.1 Sv (Fig. 6c). This OC variability is in good agreement with that estimated by S03.

Considering the MW as one of the main components of the OC system, acting as main exporter of salt at the intermediate level, we evaluate the role of each of its main branches (Figs. 6a and 7). The maximum MW_{nb} net transport takes place in summer (−1.9 ± 0.2 Sv), whereas the MW_{wb} transport is higher in spring (−0.8 ± 0.2 Sv). When the northern branch transport is smaller, the westward branch transport is higher and vice versa. On the annual scale, MW_{nb} and MW_{wb} transports are −0.9 ± 0.3 Sv and −0.4 ± 0.2 Sv, respectively, which are translated into a salt export of 33.1 ± 8 and 15.8 ± 3 Sv psu, respectively. There was no net MW transport across the limits of the southern section (within the errors bars).

The monthly time series of the MW and central water net transports are shown in Fig. 6b. A high significance correlation is found between both net transports ($r^2 = 0.90$) with 95% confidence interval (Table 2). The Gibraltar MOW (MOW and the central water inflow at Gibraltar Strait are those given by Soto-Navarro et al. (2010)) presents a maximum volume transport in April (García-Lafuente et al., 2007), representing a particular seasonal "pulse" of salty water to MW formation in the Gulf of Cadiz. The higher the net central water incoming flow and the higher the MW outflow are, the higher the OC is ($r^2 = 0.94$ for correlation for OC/central water pair, $r^2 = 0.88$ for correlation for OC/MW pair). In addition, the maximum central water entering the box during summer coincides with the maximum central water inflow through the Strait of Gibraltar, i.e., the greater the amount of central water entering the box, the greater the amount of central water entering the Strait of Gibraltar.

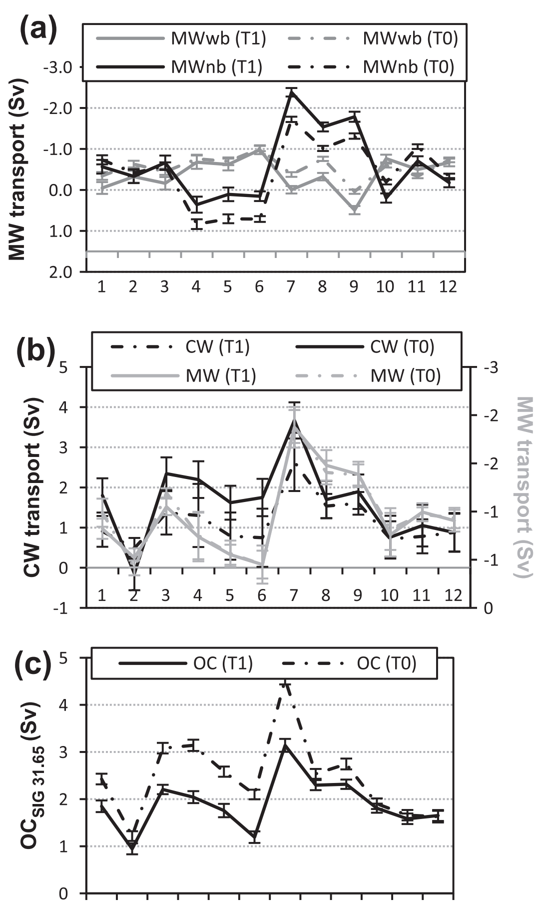

Fig. 6. Climatological monthly time series (January to December) of the main components of the OC system: (a) Westward and Northward branches of the Mediterranean Water (MW_{wb} and MW_{nb}, respectively), (b) MW and central waters net transports (whole box) and (c) overturning transport (OC).

Going further in the comprehension of the OC system, two (3D and zonal) schemes show the upper-intermediate circulation (Figs. 7 and 8, respectively). Fig. 7 complements the results described until now, providing a general perspective of the main flows at two upper (central waters) and lower (MW and AA) horizontal levels. Fig. 8 extends the results, summarizing the fluxes that take part of the OC in a simplified zonal diagram. In this figure two areas were delimited: WOA09-Box and a Gibraltar Strait box. From our results, the net Central Water transport ($MMW + ENACW_T + ENACW_P$) across the western limits of the WOA09-Box (northern, western and southern sections) was 1.4 Sv (annual mean). As the transformation of central water in intermediate water takes place within the region of the Gulf of Cadiz (Rhein and Hinrichsen, 1993; Alves et al., 2011), we assume that this net amount of Central Water would be available to reach that region and to take part in the entrainment and/or the Atlantic inflow to the Mediterranean Sea. Therefore, the entrainment (downwelling and mixing) in the Gulf of Cadiz region was approximated as the net inflow of central water into the WOA-Box, minus E–P–R over the WOA-Box superficial area and minus the central water inflow at the Gibraltar Strait. In terms of annual mean, net central water transport in the upper layer (0–500 dbar) was estimated at 2.0 ± 0.2 Sv. From the 2.0 ± 0.2 Sv of the central water net transport, 0.8 ± 0.06 Sv (Soto-Navarro et al., 2010) enters the Mediterranean Sea and thus, the rest (1.2 Sv) is destined to downwell to the intermediate layer. Part of this downwelled water recirculates without mixing with MOW (0.6 ± 0.1 Sv) and the rest (0.6 ± 0.1 Sv) would be mixed with MOW to form MW. Rhein and Hinrichsen (1993) used a local mixing model to describe the mixing of the MW undercurrent with the overlying NACW, using MOW as one end-member (13.35 °C, 38.40 psu) and a mixture of Atlantic water from different depths above the undercurrent as the other end-member. The percentage of MOW obtained from that model at 7°30'W was 34% (for MW lower core). With this dilution factor, we approximated an "expected" MW outflow (water stabilised in the Gulf of Cadiz at 1100 dbar with properties of 11.74 °C, 36.5 psu). In this approximation, we considered the mean annual MOW transport at the Gibraltar Strait (0.78 ± 0.05 Sv, Soto-Navarro et al., 2010) and took into account that 82% of this overflow comes from "pure 38.40 psu MOW", which then undergoes mixing and entrainment in the Strait (Huertas et al., 2012). The volume of MW likely to flow out of the WOA-Box with this estimation is 1.9 ± 0.2 Sv, which is in agreement with that estimated by Alves et al. (2011). The value we actually obtain is 1.2 Sv, lower than that indicated by other authors (2–3 Sv, Zenk, 1975; 1.9 Sv, Rhein and Hinrichsen, 1993; 2.3 Sv, Álvarez et al., 2005). These differences could come from the smoothed character of the climatological data. From four repeated cruises (July 1999, July 2000, November 2000, July 2001), Alves et al. (2011) estimated the entrainment of central waters at 1.2–1.7 Sv (a mean entrainment of 1.4 Sv, Fig. 8), which is closer to the climatological values taking into account that they did not differentiate between entrainment *per se* and the central water recirculation. This value is also close to those values obtained in earlier studies from Baringer and Price (1997) (1.3 Sv) or S03 (1.6 ± 0.6 Sv). Even with the summer climatology (Fig. 8, black values in brackets), when the OC appears intensified actual entrainment reaches only 1 Sv and the resulting MW outflow is 1.6 Sv. In contrast, Álvarez et al. (2005) represented an upper bound for the estimations, whose results are of the same order as Rhein and Hinrichsen (1993). Note, however, Rhein and Hinrichsen (1993) made their computations based on 1 Sv of

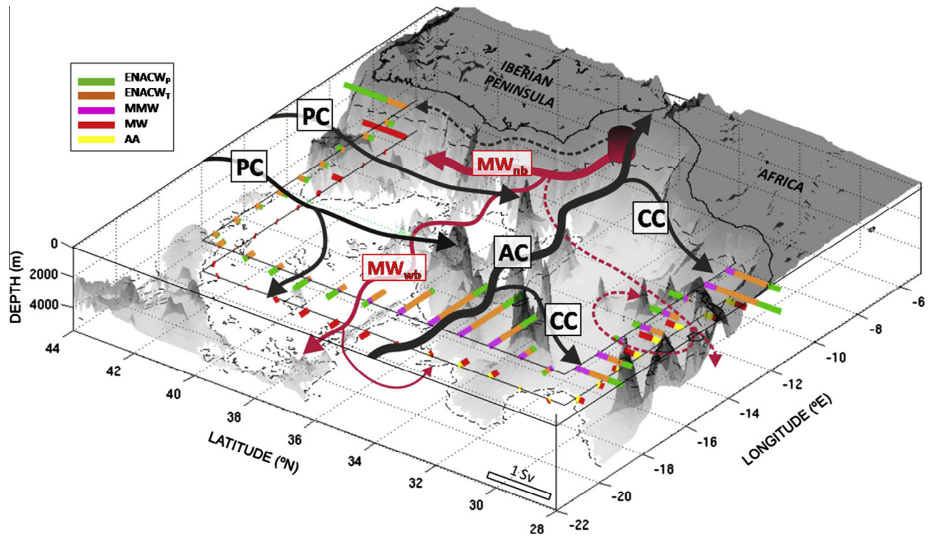

Fig. 7. Schematic diagram of the circulation of the upper-intermediate (annual mean) circulation. The principal flows at these two horizontal levels are shown with black-red arrows, respectively. Black-to-red cylinder in the Gulf of Cadiz region represents the entrainment of central waters to the Mediterranean level. Stacked coloured bars represent horizontal transports (in Sv) between node stations. In the upper level, colour bars refer to the central waters: Subpolar East North Atlantic Central Water (green), Subtropical East North Atlantic Central Water (orange) and Madeira Mode Water (pink). In the lower level, colour bars refer to Mediterranean Water (red) and Antarctic Intermediate Water (yellow).

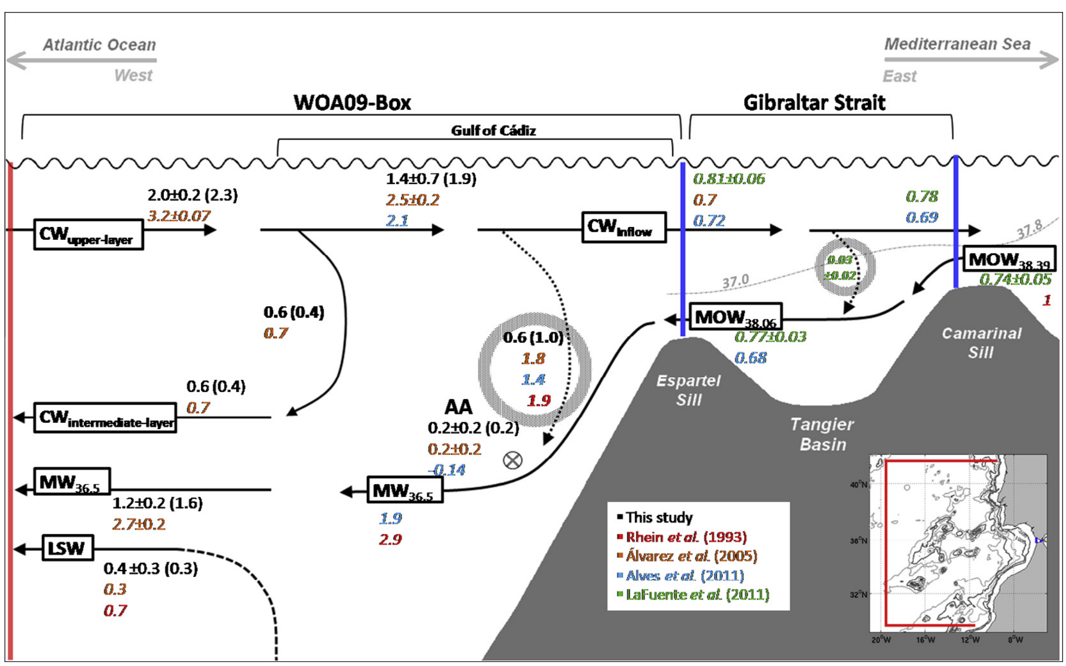

Fig. 8. Schematic summary of mean exchanges (Sv), zoomed in on the Gulf of Cadiz–Strait of Gibraltar region. Two boxes are delimited (from west to east): WOA09-Box and Gibraltar Strait box. Dotted lines and grey circles indicate areas where Central Water (CW) entrains and mixes with Mediterranean Outflow Water (MOW). Note, CW comprises the sum of the Madeira Mode Water and subtropical and subpolar types of East North Atlantic Central Water. Dashed line means Labrador Sea Water (LSW) contribution to Mediterranean Water (MW) mixing. The small crossed open circle marks the horizontal mix with the remnant Antarctic Intermediate Water (AA). Dashed–dotted thin grey line denotes the interface of zero velocity between CW-Inflow/MOW (grey numbers are the salinity values of the interface on the western and eastern sides of the strait (Huertas et al., 2012)). WOA09-Annual Climatology results are given in black numbers (WOA09-Summer values are given in parentheses) and results from the literature are in colour. Vertical axis (in metres) is illustrative (not to scale).

MOW, which nowadays is known to be too high, inflating their estimates by 30%.

4. Summary and concluding remarks

By means of an inverse box model applied to World Ocean Atlas (WOA, 2009) data, different components of the circulation in the Azores–Gibraltar Strait region were estimated, with particular focus on the mean and seasonal circulation patterns and overturning circulation system.

The upper general circulation pattern in the Azores–Madeira–Gibraltar Strait region consisted of the well-identified anticyclonic circulation cell, taking part of the broader basin-scale Subtropical Gyre with a permanent character throughout the year but slightly enhanced in spring. Seasonal mean-climatic variability of the currents system was derived. The principal currents identified from the WOA09 climatological data were the Azores Current and Azores Counter Current across the western section, the Portugal Current and the predominantly winter and autumn Iberian Poleward Current across the northern section and finally, the Canary Current across the southern section.

The annual Azores Current transport, mostly confined to the upper 1000–1500 dbar, was quantified as 6.5 ± 0.8 Sv at 19.5°W, varying seasonally from its lowest value in spring (5.3 ± 0.8 Sv), to its maximum in autumn (higher velocity maximum accompanied by a deepening and broadening of the current). The absolute maximum of the Azores Current occurs in January (10.2 ± 0.9 Sv). The Azores Counter Current appeared intensified in spring and autumn (>3 ± 0.9 Sv) with lower transports in summer and winter (< 2 ± 0.8 Sv). Autumn is the season when the Azores Counter Current becomes more easily identifiable as a westward jet. From the monthly variability of both zonal currents, we suggested a seasonally varying ratio between them with the Azores Current doubling the Counter Current in spring and autumn but with a higher-than-two ratio of the Azores Current and Azores Counter Current in summer and winter. Regarding the meridional Portugal and Canary Currents, their seasonal signal responded to favourable spring-summer Subtropical Gyre intensification and favourable upwelling conditions, exhibiting maximum transports of 5.20 ± 0.3 Sv (April) and −8.0 ± 0.4 Sv (June), respectively. In addition, as part of the Portugal Current system and reducing the net southward transport of the Portugal Current in autumn/winter, the Iberian Poleward Current was quantified at 0.2 ± 0.1 Sv with a maximum northward transport in January (1 ± 0.1 Sv); however, it was absent between the months of May to August.

The vertical structure of the circulation involved a relatively fresh upper layer of central waters flowing into the area across the northern and western WOA sections, part entraining the intermediate layer and part entering the Mediterranean Sea, together with a high-salinity intermediate layer of Mediterranean Outflow Water flowing out of the Strait of Gibraltar and ultimately, out of the WOA-Box along two principal advective (northward and westward) paths. The overturning circulation induced by the central water entrainment to the intermediate layer was quantified at 2.2 ± 0.1 Sv (annual mean), for which the magnitude was enhanced in summer (2.6 ± 0.1 Sv) and reduced by 1 Sv from autumn to spring (1.7 ± 0.2 Sv). From summer/autumn to spring, its depth decreased progressively. The density level dividing the vertical circulation structure into the upper-inflowing and lower-outflowing limbs of the overturning circulation (σ_{OC}) was identified at $\sigma_1 = 31.65$ kg m^{-3}, which is above the isopycnal that typically separates Central and Mediterranean Water ($\sigma_1 = 31.8$ kg m^{-3}).

In terms of water masses, we focused on the spread of Mediterranean water at intermediate levels and found that when the northward Mediterranean Water branch weakens in spring and autumn, the westward Mediterranean Water vein strengthens and vice versa. The maximum net transports across northern and western sections of the box were −1.9 ± 0.6 Sv (summer) and −0.8 ± 0.2 Sv (spring), respectively. The westward Mediterranean Water flow recirculates such that a more diluted form re-entered the box within the Azores Current (0.3 Sv annual mean), while the northward Mediterranean Water flow hardly recirculates within the Portugal Current (0.03 Sv annual mean). Climatically speaking, no significant (within the error 0.2 Sv) Mediterranean volume transport across the southern section was found.

The water mass composition of the principal currents was established quantitatively; the Azores Current transports mainly Central Waters (90%) with 50% comprising the subtropical variety and an increased proportion of recirculated Madeira Mode Water in summer (24%). About 40% of the Azores Counter Current corresponds to the subpolar variety of Central Waters. Other important contributors are the Mediterranean Water (25%) and the recirculated Labrador Sea Water (20%). Both the Portugal and the Canary Currents transport mainly Central Waters (>95%). During spring, the contribution of the subpolar variety to the Portugal Current exceeds that of the subtropical, whereas during the autumn-winter period, this proportion reverses. On the other hand, 60% of the Canary Current belongs to the subtropical variety, which recirculates from the Azores Current. The contribution of the Madeira Mode Water increases in autumn at the expense of the drop in the subtropical contribution.

The annual estimate for the Central Water transformation in the Gulf of Cadiz was given at 1.2 Sv. Of this, 0.6 corresponds to downwelled central water that recirculates without mixing with the underlying Mediterranean Water and the other 0.6 corresponds to central water entrainment.

To conclude, two extreme states of circulation (spring/summer vs. autumn/winter) can be described:

- On the one hand, during spring/summer, the position of the Azores High introduces a strong northerly component in the wind field over the WOA-Box region (Fig. 1). The Portugal Current and Canary Current transports reach their maximum transports in spring (absolute maximum transports in April and June, respectively), due to the enhancement of the coastal branches of both currents. Near the Gibraltar Strait, the strongest MOW flux also occurs during this period (April). In addition, the deep circulation is also slightly enhanced. The Azores Counter Current presents a relative maximum, leading to higher exportation of MW by its westward branch, while the climatological signal of the northern branch almost disappears during this season. The higher contribution of the Portugal Current to the central water net upper transport into the box makes it less saline and helps compensate for the E–P term, which is higher in late-summer early-autumn. In July, the general flow pattern in the Gulf of Cadiz is enhanced (Machín et al., 2006b) and central water inflow through the Strait of Gibraltar increases relative to the rest of the year (Soto-Navarro et al., 2010). Furthermore, in this season, we estimated that the central water net transport into the WOA-Box and the MW net outflow (northern MW branch) reach their maximum transports, leading to an increased overturning circulation (2.6 ± 0.1 Sv).
- On the other hand, in autumn, the surface circulation system appears diminished, except for the AC that presents higher transport, importing saltier central water into the box. Machín et al. (2006b) showed that higher zonal eastward transports reach the south of the Gulf of Cadiz (1 Sv of net eastward transport). As neither entrainment nor central water inflow compensates for this increased transport, the Iberian Poleward Current is expected to compensate for it. Summing up, the overturning system appears to be "relaxed" (1.7 ± 0.1 Sv).

Much effort was spent in producing time-averaged pictures, which provided a more reliable quantitative picture of the circulation than seen before. In view of the present results and conclusions, doubts over the inhomogeneity of the climatological data base (Wunsch, 1996) are assuaged by the higher quality of WOA09 and the six-fold increase in station data over previous versions (Levitus et al., 1998). In fact, currents such as the Azores Counter Current that could not be identified well by the WOA94 data (Pingree et al., 1999) can be now delimited. Nevertheless, one cannot disregard the obvious limitation of time averaging. The smoothing of the thermohaline properties maxima and the horizontal gradients reduces the geostrophic velocities by up to one order of magnitude in comparison with quasi-synoptic measurements. This fact may restrain but does not reject the particular use of WOA data to deal with water masses such as Mediterranean water, in which the (punctual) mesoscale meddy activity contributes notably to the horizontal salt fluxes. With this issue in mind, the present study illustrates a good example of how this kind of reprocessed hydrographic data can be combined with inverse methodologies (inverse box model plus multiparameter water masses analysis) leading to consistent results, as has been validated particularly in Section 3.1.1 and through the entire manuscript; thus, providing useful interpretation of the seasonal dynamics.

In further extension of this work, direct comparisons of the climatology results with a quasi-synoptic cruise for a similar box in the same area will be developed, paying attention to discrepancies in terms of horizontal salt fluxes and water masses transformations.

Acknowledgements

This work is embraced within the CAIBEX Project: *Shelf-ocean exchanges in the Canaries-Iberia Large Marine Ecosystem* (CTM2007-66408-C02/MAR), supported by the Spanish Council of Education and Science. The first author is funded by a predoctoral fellowship (FPU) of the Formation National Program of Human Resources, within the framework of the National Plan of Scientific Investigation, Development and Technologic Innovation 2008–2011, from the Spanish Council of Education. Thank you very much to Professor E.D. Barton for his invaluable help with the English review. We also thank the editor and the two anonymous reviewers for their helpful comments and suggestions, which have greatly contributed to improve the original manuscript.

References

Álvarez, M., 2002.Water Masses and Transports of Physical and Chemical Properties in the Subpolar North Atlantic Gyre. Ph.D. Thesis, University of Vigo, Spain, Unpublished.

Álvarez, M., Álvarez-Salgado, X.A., 2009. Chemical tracer transport in the eastern boundary current system of the North Atlantic. Ciencias Marinas 35, 123–139.

Álvarez, M., Pérez, F.F., Shoosmith, D.R., Bryden, H., 2005. Unaccounted role of Mediterranean Water in the drawdown of anthropogenic carbon. Journal of Geophysical Research 110, C09S03. http://dx.doi.org/10.1029/2004JC002633.

Álvarez-Salgado, Figueiras, F.G., Perez, F.F., Groom, S., Nogueira, E., Borges, A.V., Chou, L., Castro, C.G., Moncoiffe, G., Ríos, A.F., Miller, A.E.J., Frankignoulle, M., Savidge, G., Wollast, R., 2003. The Portugal coastal counter current off NW Spain: new insights on its biogeochemical variability. Progress in Oceanography 56, 281–321.

Alves, M., Gaillard, F., Sparrow, M., Knoll, M., Giraud, S., 2002. Circulation patterns and transport of the Azores Front-Current system. Deep-Sea Research 49 (19), 3983–4002.

Alves, M., Carton, X., Ambar, I., 2011. Hydrological structure, circulation and water mass transport in the Gulf of Cadiz. International Journal of Geoscience 2, 432–456.

Ambar, I., Howe, M.R., 1979a. Observations of the Mediterranean outflow – I: mixing in the Mediterranean outflow. Deep-Sea Research Part I 26A, 535–554.

Ambar, I., Howe, M., 1979b. Observations of the Mediterranean outflow – II: the deep circulation in the vicinity of the Gulf of Cadiz. Deep-Sea Research Part I 26A, 555–568.

Ambar, I., Armi, L., Bower, A., Ferreira, T., 1999. Some aspects of time variability of the Mediterranean Water off South Portugal. Deep-Sea Research Part I 46, 1109–1136.

Antonov, J.I., Seidov, D., Boyer, T.P., Locarnini, R.A., Mishonov, A.V., Garcia, H.E., Baranova, O.K., Zweng, M.M., Johnson, D.R., 2010. In: Levitus, S. (Ed.), World Ocean Atlas 2009: Salinity, vol. 2. NOAA Atlas NESDIS 69, U.S. Gov. Printing Office, Washington, DC, 184 pp.

Arhan, M.A., Colin de Verdière, A., Memery, L., 1994. The eastern boundary of the subtropical North Atlantic. Journal of Physical Oceanography 24, 1295–1316.

Armi, L., Hebert, D., Oakey, N., Price, J.M., Richarson, P.L., Rossby, H.T., Ruddick, B., 1989. Two years in the life of a Mediterranean salt lens. Journal of Physical Oceanography 19, 354–370.

Baringer, M., Price, J.F., 1997. Mixing and spreading of the Mediterranean outflow. Journal of Physical Oceanography 27, 1654–1677.

Barton, E.D., 1998. Eastern boundary of the North Atlantic: Northwest Africa and Iberia. In: Brink, K.H., Robinson, A.R. (Eds.), The Sea. The Global Coastal Ocean: Regional Studies and Syntheses, vol. 11. Harvard Univ. Press, New York, pp. 633–657 (Chapter 22).

Barton, E.D., 2001. Ocean Currents: Atlantic Eastern Boundary – Canary Current/ Portugal Current. In: Steele, J., Thorpe, S., Turekian, K. (Eds.), Encyclopaedia of Ocean Sciences, vol. 1. Academic Press, London, pp. 380–389.

Bower, A.S., Armi, L., Ambar, I., 1995. Direct evidence of meddy formation off the southwestern coast of Portugal. Deep-Sea Research Part I 42, 1621–1630.

Bower, A.S., Armi, L., Ambar, I., 1997. Lagrangian observations of meddy formation during a Mediterranean Undercurrent Seeding Experiment. Journal of Physical Oceanography 27, 2545–2575.

Boyer, T.P., Antonov, J.I., Baranova, O.K., Garcia, H.E., Johnson, D.R., Locarnini, R.A., Mishonov, A.V., O'Brien, T.D., Seidov, D., Smolyar, I.V., Zweng, M.M., 2009. In: Levitus, S. (Ed.), World Ocean Database 2009. Introduction, NOAA Atlas NESDIS 66, U.S. Gov. Printing Office, Washington, DC, 216 pp. (Chapter 1)

Carracedo, L.I., Pardo, P.C., Villacieros-Robineau, N., De la Granda, F., Gilcoto, M., Pérez F.F., 2012. Temporal changes of the water masses distribution and transports along the 20°W CAIBOX section (NE Atlantic). Ciencias Marinas 38(1B), 263–286.

Comas-Rodríguez, I., Hernández-Guerra, A., Fraile-Nuez, E., Martínez-Marrero, A., Benítez-Barrios, V.M., Pérez-Hernández, M.D., Vélez-Belchí, P., 2011. The Azores Current System from a meridional section at 24.5°W. Journal of Geophysical Research 116, C09021. http://dx.doi.org/10.1029/2011JC007129.

Criado-Aldeanueva, F., García-Lafuente, J., Vargas, J.M., Del Río, J., Vázquez, A., Reul, A., Sánchez, A., 2006. Distribution and circulation of water masses in the Gulf of Cadiz from in situ observations. Deep-Sea Research Part II 53, 1144–1160.

Dickson, R.R., Gould, W.J., Muller, T.J., Maillard, C., 1985. Estimates of the mean circulation in the deep (>2000 m) layer of the Eastern North Atlantic. Progress in Oceanography 14, 103–127.

Fajar, N.M., Pardo, P.C., Carracedo, L.I., Vázquez-Rodríguez, M., Ríos, A.F., Pérez, F., 2012. Trends of the anthropogenic CO_2 along 20°W in the Iberian Basin. Ciencias Marinas 38 (1B), 287–306.

Fraile-Nuez, E., Machín, F., Vélez-Belchí, P., López-Laatzen, F., Borges, R., Benítez-Barrios, V., Hernández-Guerra, A., 2010. Nine years of mass transport data in the eastern boundary of the North Atlantic Subtropical Gyre. Journal of Geophysical Research 115, C09009. http://dx.doi.org/10.1029/2010JC006161.

Frouin, R., Fiúza, A.F.G., Ambar, I., Boyd, T.J., 1990. Observations of a poleward surface current off the coasts of Portugal and Spain during winter. Journal of Geophysical Research 95, 679–691.

Fusco, G., Artale, V., Cotroneo, Y., Sannino, G., 2008. Thermohaline variability of Mediterranean Water in the Gulf of Cadiz: 1948–1999. Deep-Sea Research Part I 55, 1624–1638.

Ganachaud, A., Wunsch, C., 2000. Improved estimates of global ocean circulation, heat transport and mixing from hydrographic data. Nature 408, 453–457.

Ganachaud, A., Wunsch, C., Marotzke, J., Toole, J., 2000. Meridional overturning and large-scale circulation of the Indian Ocean. Journal of Geophysical Research 105, 26117–26134.

García-Lafuente, J., Sánchez-Román, A., Díaz del Río, G., Sannino, G., Sánchez-Garrido, J.C., 2007. Recent observations of seasonal variability of the Mediterranean outflow in the Strait of Gibraltar. Journal of Geophysical Research 112, C10005. http://dx.doi.org/10.1029/2006JC003992.

Haynes, R., Barton, E.D., 1990. A poleward flow along the Atlantic coast of the Iberian Peninsula. Journal of Geophysical Research 95, 11425–11441.

Hernandez-Guerra, A., Fraile-Nuez, E., Lopez-Laatzen, R.E., Martínez, A., Parrilla, G., Vélez-Belchí, P., 2005. Canary Current and North Equatorial Current form an inverse box model. Journal of Geophysical Research 110, C12019. http://dx.doi.org/10.1029/2005JC003032.

Huertas, I.E., Ríos, A.F., García-Lafuente, J., Navarro, G., Makaoui, A., Sánchez-Román, A., Rodriguez-Galvez, S., Orbi, A., Ruíz, J., Pérez, F.F., 2012. Atlantic forcing of the Mediterranean oligotrophy. Global Biogeochemical Cycles 26, GB2022. http://dx.doi.org/10.1029/2011GB004167.

Jia, Y., 2000. Formation of an Azores Current due to Mediterranean overflow in a modelling study of the North Atlantic. Journal of Physical Oceanography 30, 2342–2358.

Karstensen, J., Tomczak, M., 1998. Age determination of mixed water masses using CFC and oxygen data. Journal of Geophysical Research 103, 18599–18610.

Kida, S., Price, J.F., Yang, J., 2008. The upper-oceanic response to overflows: a mechanism for the Azores Current. Journal of Physical Oceanography 38, 880–895.

Klein, B., Siedler, G., 1989. On the origin of the Azores Current. Journal of Geophysical Research 94, 6159–6168.

Levitus, S., Boyer, T.P., Conkright, M.E., O'Brien, T., Antonov, J., Stephens, C., Stathoplos, L., Johnson, D., Gelfeld, R., 1998. In: Levitus, S. (Ed.), World Ocean Database 1998. Introduction, vol. 1. NOAA Atlas NESDIS 18, U.S. Gov. Printing Office, Washington, DC, 346 pp.

Lherminier, P., Mercier, H., Gourcuff, C., Alvarez, M.F., Bacon, S., Kermabon, C., 2007. Transport across the 2002 Greenland-Portugal section and comparison with 1997. Journal of Geophysical Research 112, C07003. http://dx.doi.org/10.1029/2006JC003716.

Lherminier, P., Mercier, H., Huck, T., Gourcuff, C., Pérez, F.F., Morin, P., Sarafanov, A., Falina, A., 2010. The Atlantic Meridional Overturning Circulation and the subpolar gyre at the A25-OVIDE section in June 2002 and 2004. Deep-Sea Research Part I 57 (11), 1374–1391.

Locarnini, R.A., Mishonov, A.V., Antonov, J.I., Boyer, T.P., Garcia, H.E., Baranova, O.K., Zweng, M.M., Johnson, D.R., 2010. In: Levitus, S. (Ed.), World Ocean Atlas 2009. Temperature. NOAA Atlas NESDIS 68, vol. 1. U.S. Gov. Printing Office, Washington, DC, 184 pp.

Louarn, E., Morin, P., 2011. Antarctic Intermediate Water influence on Mediterranean Sea Water outflow. Deep-Sea Research Part I 58 (9), 932–942. http://dx.doi.org/10.1016/j.dsr.2011.05.009.

Lux, M., Mercier, H., Arhan, M., 2001. Inter hemispheric exchanges of mass and heat in the Atlantic Ocean in January–March 1993. Deep-Sea Research Part I 48 (3), 605–638.

Machín, F., Pelegrí, J.L., 2009. Northward penetration of Antarctic intermediate water off Northwest Africa. Journal of Physical Oceanography 39, 512–535.

Machín, F., Hernández-Guerra, A., Pelegrí, J.L., 2006a. Mass fluxes in the Canary Basin. Progress in Oceanography 70, 416–447.

Machín, F., Pelegrí, J.L., Marrero-Díaz, A., Laiz, I., Ratsimandresy, A.W., 2006b. Near-surface circulation in the southern Gulf of Cadiz. Deep-Sea Research Part II 53, 1161–1181.

Mazé, J.P., Arhan, M., Mercier, H., 1997. Volume budget of the eastern boundary layer off the Iberian Peninsula. Deep-Sea Research Part I 44, 1543–1574.

McCartney, M.S., 1992. Recirculating components to the deep boundary current of the northern North Atlantic. Progress in Oceanography 29, 283–383.

McCartney, M.S., Bennet, S.L., Woodgate-Jones, M.E., 1991. Eastward flow through the Mid-Atlantic Ridge at 11°N and its influence on the abyss of the Eastern Basin. Journal of Physical Oceanography 21, 1081–1121.

Mercier, H., 1986. Determining the general circulation of the ocean: a non linear inverse problem. Journal of Geophysical Research 91 (C4), 5103–5109.

Navarro-Pérez, E., Barton, E.D., 2001. Seasonal and interannual variability of the Canary Current. Scientia Marina 65, 205–213.

New, A.L., Jia, Y., Coulibaly, M., Dengg, J., 2001. On the role of the Azores Current in the ventilation of the North Atlantic Ocean. Progress in Oceanography 48, 163–194.

Onken, R., 1992. The Azores Countercurrent. Journal of Physical Oceanography 23, 1638–1646.

Paillet, J., Mercier, H., 1997. An inverse model of the eastern North Atlantic general circulation and thermocline ventilation. Deep-Sea Research 44 (8), 1293–1328.

Pardo, P.C., Pérez, F.F., Velo, A., Gilcoto, M., 2012. Water masses distribution in the Southern Ocean: improvement of an extended OMP (eOMP) analysis. Progress in Oceanography 103, 92–105.

Péliz, A., Dubert, J., Haidvogel, D.B., LeCann, B., 2003. Generation and unstable evolution of a density-driven Eastern Poleward Current: the Iberian Poleward Current. Journal of Geophysical Research 108 (C8), 3268. http://dx.doi.org/10.1029/2002JC001443.

Péliz, A., Dubert, J., Santos, A.M.P., Oliveira, P.B., LeCann, B., 2005. Winter upper ocean circulation in the western Iberian basin, fronts, eddies and poleward flows: an overview. Deep-Sea Research Part I 52 (4), 621–646.

Péliz, A., Marchesiello, P., Santos, A.M.P., Dubert, J., Teles-Machado, A., Marta-Almeida, M., Le Cann, B., 2009. Surface circulation in the Gulf of Cadiz: 2. Inflow-outflow coupling and the Gulf of Cadiz slope current. Journal of Geophysical Research 114, C03011. http://dx.doi.org/10.1029/2008JC004771.

Pérez, F.F., Mintrop, L., Llina, O., González-Dávila, M., Castro, C., Álvarez, M., Körtzinger, A., Santana-Casiano, M., Rueda, M.J., Ríos, A.F., 2001. Mixing analysis of nutrients, oxygen and inorganic carbon in the Canary Islands Region. Journal of Marine Systems 28 (3–4), 183–201.

Pérez, F.F., Gilcoto, M., Ríos, A.F., 2003. Large and mesoscale variability of the water masses and the deep chlorophyll maximum in the Azores Front. Journal of Geophysical Research 108 (C7), 3215–3233.

Pingree, R.D., Garcia-Soto, C., Sinha, B., 1999. Position and structure of the Subtropical/Azores Front region from combined Lagrangian and remote sensing (IR/altimeter/SeaWiFS) measurements. Journal of Marine Biological Association of the UK 79, 769–792.

Polzin, K.L., Toole, J.M., Ledwell, J.R., Schmitt, R.W., 1997. Spatial variability of turbulent mixing in the Abyssal Ocean. Nature 276, 93–96.

Reid, J.L., 1994. On the total geostrophic circulation of the North Atlantic Ocean: flow patterns, tracers, and transports. Progress in Oceanography 33, 1–92.

Rhein, M., Hinrichsen, H.H., 1993. Modification of Mediterranean Water in the Gulf of Cadiz, studied with hydrographic, nutrient and chlorofluoromethane data. Deep-Sea Research Part I 40 (2), 267–291.

Richardson, P.L., Bower, A.S., Zenk, W., 2000. A census of Meddies tracked by floats. Progress in Oceanography 45, 209–250.

Ríos, A.F., Pérez, F.F., Fraga, F., 1992. Water masses in the upper and middle North Atlantic Ocean east of the Azores. Deep-Sea Research Part II 39 (3/4), 645–658.

Saunders, P.M., 1982. Circulation in the eastern North Atlantic. Journal of Marine Research 40, 641–657.

Shapiro, G.I., Meschanov, S.L., 1996. Spreading pattern and mesoscale structure of Mediterranean outflow in the Iberian Basin estimated from historical data. Journal of Marine Systems 7, 337–348.

Siedler, G., Kuhl, A., Zenk, W., 1987. The Madeira mode water. Journal of Physical Oceanography 17, 1561–1970.

Slater, D.R., 2003. The Transport of Mediterranean Water in the North Atlantic Ocean. Ph.D. Thesis, University of Southampton, UK, Unpublished.

Smith, R.D., Maltrud, M.E., 1999. Numerical simulation of the North Atlantic Ocean at 1/10. Journal of Physical Oceanography 30, 1532–1561.

Soto-Navarro, J., Criado-Aldeanueva, F., García-Lafuente, J., Sánchez-Román, A., 2010. Estimation of the Atlantic inflow through the Strait of Gibraltar from climatological and in situ data. Journal of Geophysical Research 115, C10023. http://dx.doi.org/10.1029/2010JC006302.

Stramma, L., Siedler, G., 1988. Seasonal changes in the North Atlantic subtropical gyre. Journal of Geophysical Research 93, 8111–8118.

Tsuchiya, M., Talley, L.D., McCartney, M.S., 1992. An eastern Atlantic section from Iceland southward across the equator. Deep-Sea Research Part I 39, 1885–1917.

van Aken, H.M., 2000a. The hydrography of the mid-latitude northeast Atlantic Ocean. I: the deep water masses. Deep-Sea Research Part I 47 (5), 757–788.

van Aken, H.M., 2000b. The hydrography of the mid-latitude northeast Atlantic Ocean II: the intermediate water masses. Deep-Sea Research Part I 47 (5), 789–824.

Wunsch, C., 1977. Determining the general circulation of the oceans: a preliminary discussion. Science 196, 871–875.

Wunsch, C., 1978. The North Atlantic general circulation West of 50°W determined by inverse methods. Reviews of Geophysics and Space Physics 16, 583–620.

Wunsch, C., 1996. The Ocean Circulation Inverse Problem. Cambridge University Press, Cambridge.

Zenk, W., 1975. On the Mediterranean outflow west of Gibraltar. Meteor Forschungsergeb 16, 23–24.